Article

Data-Driven Discovery of a New Fluorescent BASHY Dye for Bioimaging

João M.J.M. Ravasco, João Felicidade, Maria V. Pinto, Fábio M.F. Santos, René Campos-González, Jesús F. Arteaga, Manon Mehraz, Christelle Langevin, Adelaide Fernandes, Ha-Chi Nguyen, David Y.W. Ng, Jaime A.S. Coelho,* Uwe Pischel,* and Pedro M.P. Gois*

Read Online

ACCESS | Metrics & More | Article Recommendations | SI Supporting Information

ABSTRACT: Fluorescent molecules play a crucial role in biomedicine by facilitating the visualization and tracking of biological processes with sensitivity and specificity. However, tailoring their structure to meet the demands of live cell and *in vivo* imaging presents a significant challenge due to the intricate interplay of factors governing their structural and photophysical properties. In this study, we explored the potential of using multivariate linear free-energy relationships (mLFER) to optimize a multicomponent fluorescent platform. We prepared a small library of 20 fluorescent boronic-acid-derived salicylidenehydrazone (BASHY) complexes using a versatile reaction protocol and characterized their chemical stability in water-containing media. The obtained data served as input for the development of an mLFER model, enabling the prediction of a new BASHY dye and unraveling previously unknown mechanisms governing the stability of this unique platform of fluorescent dyes. The optimized dye was successfully employed in live cell experiments and in zebrafish larvae.

KEYWORDS: *boronic acids, BASHY dyes, mLFER, bioimaging, FLIM, zebra fish*

INTRODUCTION

Fluorescent dyes are a highly valuable class of functional molecules, extensively used to interrogate the complexity of biological processes.[1−5] In recent years, many efforts have been made to expand the chemical space of these compounds, namely by designing chromophores with structural and photophysical properties tailored for bioimaging.[6−22] In this quest, the diversification of the dye architecture is frequently necessary to meet the biological requirements of the specific application. However, this may be a particularly difficult task, since molecular diversification often interferes with the electronic structure and thus, the photophysical properties of the chromophore. Hence, the discovery of synthetic methods to generate easily tunable dyes with predictable fluorescence properties is pivotal to support the imaging of complex biological processes.

In this context, the high structural diversity offered by multicomponent reactions (MCRs) can be a particularly useful strategy to discover and diversify functional fluorescent molecules.[23,24] However, while the current use of MCRs has resulted in the facile conjugation of chromophores to other functional units,[25] the application of these reactions in the discovery and optimization of chromophores, has been far less explored.[26,27] This lack arises from the fact that very few MCRs generate fluorescent cores with suitable properties to be used as dyes.

An interesting example for an MCR-based fluorophore family is the BASHY (boronic-acid derived salicylidenehydrazone) dye platform.[28−34] These chromophores show bright ($\varepsilon \times \Phi_f$ of up to 40000 $M^{-1}cm^{-1}$) and environmentally responsive emission in the green-to-red spectral range (emission maxima between 510 and 620 nm). However, their use in bioimaging applications of more complex biological systems has been limited by their suboptimal hydrolytic stability under physiological conditions.

Foreseeable, the hydrolytic stability of the BASHY dyes is guided by an intricate pattern of interconnected electronic and steric factors. Therefore, dye optimization would benefit from a rational design that goes far beyond a trial-and-error based

approach. Data science and artificial intelligence, including machine learning, are powerful tools to accelerate development in several applications within the broad field of organic chemistry.[35−39] Specifically, multivariate linear free-energy relationships (mLFER), using physical-organic molecular descriptors, have been applied quantitatively to describe and predict mechanistic nuances and reactivity patterns of complex chemical structures.[40,41] This has been used successfully in the context of organic reactivity,[42−47] catalyst design/catalytic processes,[48−53] and occasionally in the prediction of optical spectroscopic properties of chromophores.[54] In the present work we demonstrate that the mLFER approach is suited for the design and fundamental understanding of a BASHY lead structure (see Figure 1), featuring photophysical properties and hydrolytic stability in accordance with the demands of live cell and *in vivo* imaging studies.
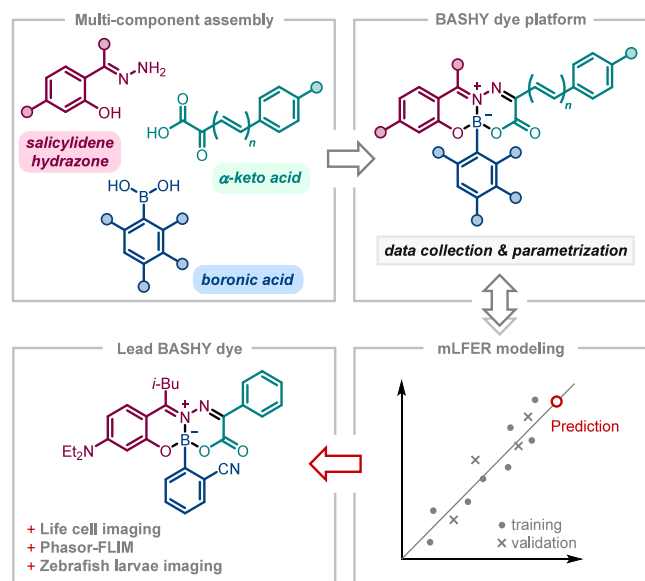

Figure 1. Workflow for the discovery of optimized BASHY dyes, using multivariate linear free energy relationships (mLFER).

■ RESULTS AND DISCUSSION

Based on our previous experience with the BASHY platform and the main factors that govern the fluorescence characteristics, the following inputs were employed to narrow down the vast potential pool of dyes. *i*) Dyes with a strong electron-donor group (substituent R^2; Scheme 1) were considered.[28,33] This setting has been shown previously to possess the most appealing photophysical properties in the context of a push–pull mechanism (fluorescence extending to the green-to-red spectral window, strong solvatofluorochromism). *ii*) Extension of the salicylidenehydrazone axis with one or two conjugated exocyclic double bonds leads to further red-shift of the absorption and fluorescence features, according to cyanine-like excited-state characteristics.[31,55] *iii*) The modification on the "vertical positions", i.e., alkylation at the iminium carbon (substituent R^1; Scheme 1) and the use of a substituted phenylboronic acid component (substituents R^3; Scheme 1) are known to have generally none or only minor influence on the fluorescence properties of the dyes.[29,34] With these fundamental concepts, a series of compounds with ample

Scheme 1. Construction of a Small Library of BASHY Dyes[a]
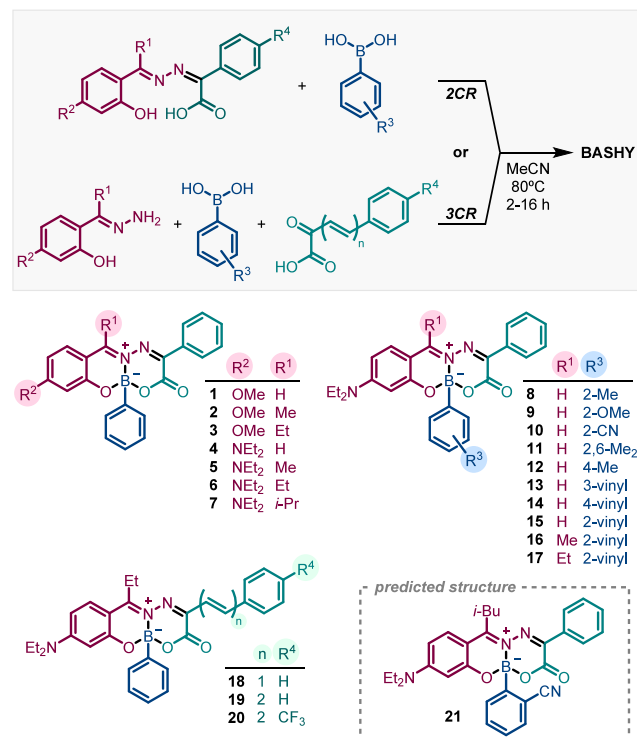
[a]See details in the Supporting Information and in refs 28 and 31.

variation of electronic and steric properties, but highly predictable photophysical characteristics was designed.

Building on the multicomponent modularity of BASHY dyes, a small library of 20 members was prepared (Scheme 1), which forms the initial chemical space of our optimization study. The dyes contain electron donors (i.e., MeO or Et_2N) at the R^2 position and alkyl substituents of varying electronic and steric demand at the R^1 position (Me, Et, *i*-Pr). Further, the phenyl ring of the boronic acid component was decorated with groups (R^3) of varying steric demand (e.g., 2-Me, 2-OMe, 2,6-Me_2, 2-vinyl). The compounds were synthesized according to our previously reported reaction protocol[28] and were obtained in generally very good to excellent chemical yields. However, bulky *ortho*-substituents on arylboronic acids and isopropyl alkylation at the iminium carbon resulted in somewhat reduced chemical yields (<50%; see the Supporting Information).

The main photophysical properties of the small library of BASHY dyes are compiled in the Supporting Information. For experimental convenience these data were collected in toluene, as it guarantees solubility and high chemical stability across the complete set of compounds. Albeit these conditions do not reflect the intended use of the optimized lead dye under physiological conditions, it provides an informative snapshot of the general photophysical trends that are observed in the synthesized library. These observations are in conformity with the previously drawn conclusions about the photophysical scope of the BASHY platform (see above).[28,29,31] As opposed to the optoelectronic properties, the structurally and electronically diverse nature of the investigated set of BASHY dyes is clearly visible in the differentiated hydrolytic stability, resulting in half-lives ranging from 2 to 6175 min ($t_{1/2}$; see the Supporting Information). This parameter was evaluated in buffered aqueous solutions, containing some organic cosolvent

for solubility reasons. The obtained half-lives were then converted into the corresponding Gibbs free energies of activation, which span from 20 to 25 kcal mol^{-1} (see the Supporting Information). This provided the relative hydrolytic reactivity of the dyes under nonphysiological, but consistent conditions, enabling us to identify a lead candidate by mLFER that could then be further tested under more biorelevant conditions (see below).
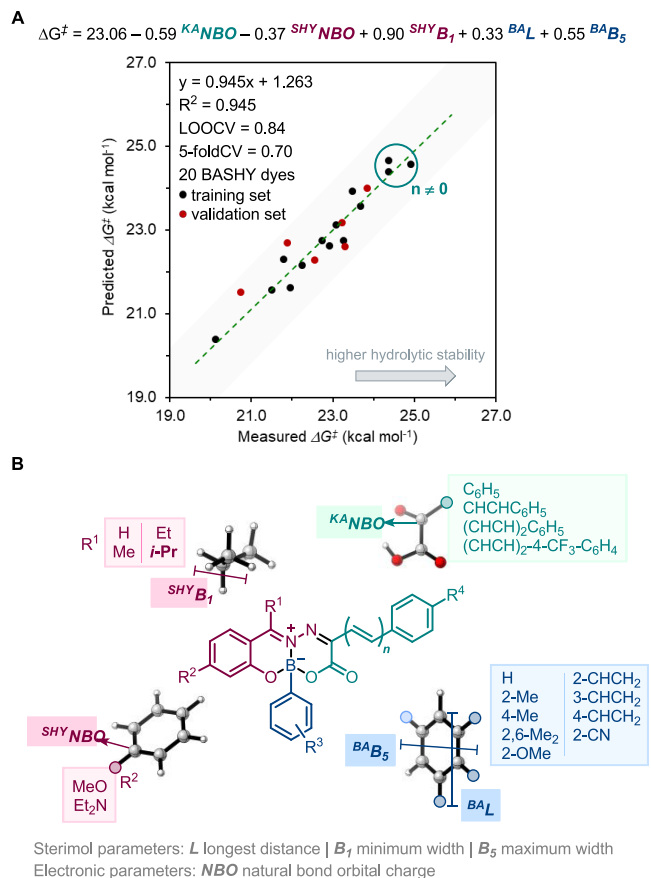
To account for the factors that govern hydrolysis and to arrive at pinpointed predictions of water-stable BASHY dyes, we performed a multivariate linear regression analysis on the data set employing DFT-calculated descriptors, such as steric (Sterimol L, B_1, and B_5, being the length, minimum and maximum width of a particular substituent, respectively) and electronic parameters (NBO charges); see Figure 2. To

Figure 2. (A) Multivariate model for BASHY hydrolysis. (B) Parameters and visual analysis of the model terms contributions to $\Delta G^{\ddagger}$. SHY: salicylidenehydrazone, KA: α-ketoacid, BA: boronic acid.

diminish the computational cost and exclude the dependence of these descriptors on conformational variations of the BASHY structure, we obtained them directly from truncated models of the three individual components that merge into the BASHY architecture (see Figure 2B and the Supporting Information for more details).

The multivariate linear regression analysis of a pseudorandomly generated training set of 14 BASHY dyes produced a model featuring *i*) electronic parameters of the substituents responsible for the push−pull mechanism and *ii*) steric parameters of the substituents R^1 and R^3 at the "vertical positions". The goodness-of-fit R^2 of 0.94 points to a highly

significant correlation between the selected descriptors and the hydrolytic stability (Figure 2A). Further, our confidence level into the developed mLFER model and its predictive robustness was reinforced by evaluating an external validation set (consisting of six dyes that were not included in the training set) and standard cross-validation analysis, which yielded consistently good scores ($R^2_{\text{validation}}$ = 0.82, LOOCV = 0.84, and 5-foldCV = 0.70).

Noteworthy, parameters of all considered structural fragments (see Figure 2B) were found to be statistically relevant for framing the hydrolytic stability of the dyes. This quantitative observation corroborates the need for a holistic approach toward BASHY probe design and stresses the importance of having access to the fluorophore platform in a versatile synthetic protocol, thereby allowing the straightforward and systematic modification of the BASHY core.

From the multivariate model (Figure 2A) it can be observed that the most relevant electronic factors, ^{KA}NBO and ^{SHY}NBO, correlate negatively with $\Delta G^{\ddagger}$, suggesting that electron-donor substitution (R^2) and a less electrophilic α-keto acid (KA) component improve the hydrolytic stability. The electronic manipulation of the phenyl boronic acid component is not expected to affect the hydrolytic hotspots of the BASHY dye. This is because the boron-appended aryl residue is electronically decoupled from the rest of the BASHY skeleton, being oriented out of the plane of the salicylidenehydrazone backbone. Hence, modifications at this moiety can be used to introduce protective steric modulation with generally negligible effects on the photophysical properties of the chromophore itself (see data in the Supporting Information). Indeed, the Sterimol B_1 (iminium substituent R^1) as well as B_5 and L (referring to the boronic acid component) correlate positively with hydrolytic resistance. We postulate that the steric conflict between the *ortho*-substitution on the phenyl ring that is introduced with the boronic acid component and the bulky salicylidenehydrazone scaffold might contribute to steric/hydrophobic shielding of the hydrolytic hotspots (see below for DFT calculations on the optimized dye **21**). A possible common hydrophobic protective mechanism involving aryl *ortho*-substitution and alkylation at the iminium carbon can be suggested by the discrete improvement of the stability upon alkylation of the salicylidenehydrazone in dye **15** versus **17** (~2.7-fold improvement) or dye **4** versus **6** (~30-fold). However, the combination of both strategies provides synergistic effects, thus, suggesting the involvement of additional factors.
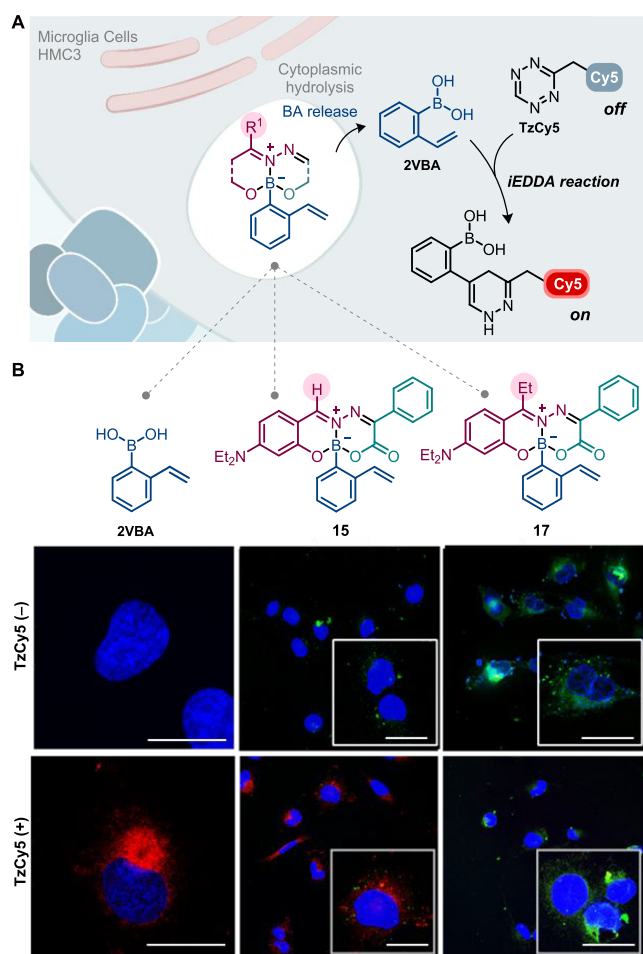
To validate the importance of such synergistic stability enhancement, we tested BASHY scaffolds in a cellular environment. To this end, we developed a direct dual-color imaging assay to detect BASHY hydrolysis *in cellulo* (see Figure 3A). This assay is based on the inverse electron-demand Diels−Alder (iEDDA) reaction of a Cy5-labeled tetrazine (TzCy5) with 2-vinylboronic acid (2VBA). Using a previously reported multivariate model, trained to predict iEDDA reactivity,[42] we identified the dyes **15** and **17** as effective bioorthogonal cages (low reactivity toward tetrazines due to the spatial proximity of the small vinyl rest and the bulky salicylidenehydrazone backbone of the dyes) and 2VBA as an adequate dienophile; see experimental verification in the Supporting Information. On hydrolysis of the BASHY dyes, 2VBA is released and the subsequent iEDDA reaction should trigger an ON-switching of the fluorescence of the Cy5 label (Figure 3A).

Figure 3. (A) Working principle of the fluorescence assay for following the hydrolysis of BASHY in cellular environments. HMC3 microglial cells (nuclear stain DAPI, blue) were cultured for 24 h and subsequently incubated with (B) 2VBA (positive control) or BASHY dyes **15** and **17** (green) for 1 h, after which they were incubated with TzCy5 for another hour. Representative images showing a marked turn-on of Cy5 (red) in the presence of 2VBA, an evident TzCy5 reaction in the presence of BASHY dye **15**, and an only minor turn-on effect in the presence of BASHY dye **17**. Scale bar: 25 μm.

HMC3 microglial cells were selected for this study, due to their capacity to effectively internalize BASHY dyes.[32] The incubation of the BASHY dyes **15** or **17** in HMC3 microglial cells followed by incubation with TzCy5 highlighted the influence of BASHY stability on their bioimaging suitability. BASHY dye **15** showed a notable Cy5 turn-on response (Figure 3B), corroborating the significant hydrolysis of the dye, accompanied by the release of 2VBA. In contrast, the hydrolytically more stable BASHY **17** (see data in the Supporting Information) showed remarkably low tetrazine reactivity (Figure 3B) and hence, no red Cy5 emission was detected.

Considering these results, we strived to apply the mLFER model for the prediction of a new lead BASHY dye with sufficient hydrolytically stability. BASHY dye **21** (see Scheme 1), featuring an isobutyl substituent as R^1 and a nitrile group in the *ortho*-position of the phenylboronic acid component (R^3), was predicted as potential hit. This dye is expected to display the highest $\Delta G^{\ddagger}$ calculated for this series ($\Delta G^{\ddagger}$ = 23.83 kcal mol^{-1}) and was synthesized in high chemical yield (see the

Supporting Information). Having dye **21** at hand, its hydrolytic stability was evaluated in aqueous solution (PBS, pH 7.4), containing 5% (v/v) DMF as cosolvent. Under these specific conditions, the dye features a significant hydrolytic stability, characterized by a half-life of 95 h. This corresponds to $\Delta G^{\ddagger}_{exp}$ = 24.85 kcal mol^{-1}, which agrees within error limit with the value predicted by mLFER (see above). In addition, the stability of **21** in human blood plasma (no degradation during a 70-h observation range) and in Dulbecco's Modified Eagle Medium (DMEM; half-life of 128 h) points to an elevated biocompatibility of the dye.

On a side note, **21** practically equals the performance of dye **20**, which was included in the original library. However, dye **21** features less rotational freedom than **20**, disfavoring non-radiative deactivation of its excited state. In addition, dye **20** populates the excited triplet state to a significant extent.[56] This is showcased by a significantly higher fluorescence quantum yield and lifetime of **21** as compared to **20** (see data in the Supporting Information).

The significant hydrolytic stability of **21** was rationalized by transition state analysis using density functional theory (DFT). Intuitively, the iminium carbon (*a*), along with the imine (*b*) and the carboxylate (*c*) carbons are predicted to be susceptible to the nucleophilic attack of water (see assignments in upper left structure in Figure 4). Computational studies of Fukui
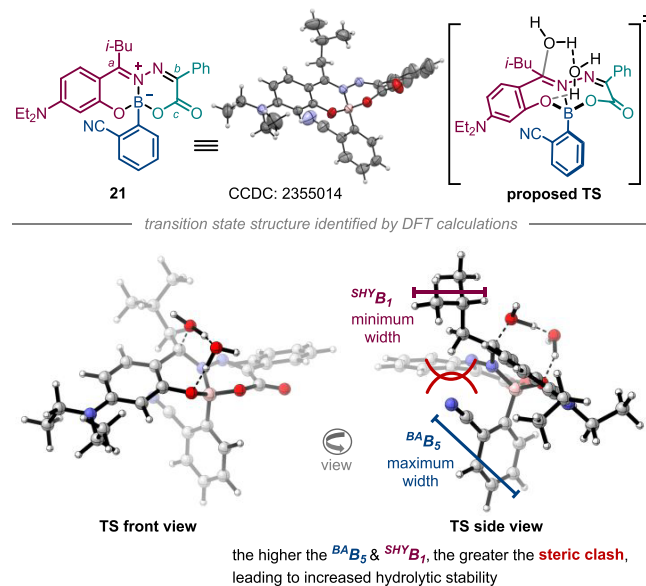
Figure 4. DFT-optimized transition state structure for the attack of water at the iminium carbon in dye **21** and implications of some parameters from data analysis on the hydrolytic stability. In the upper part also the crystal structure of **21** is shown.

indices f^+ show that the carbon atom (*a*) is the most electrophilic site in the dye [f^+: 0.21 (*a*), 0.16 (*b*), 0.00 (*c*)]. The transition state structure for the attack of water at the iminium carbon (using an H-bonded dimer of water molecules to facilitate proton transfer), computed at M06-2X/def2-TZVPP/PCM-SMD(water)//M06-2X/6-31G(d,p) level of theory, is depicted in Figure 4. Similar transition states were located for other model nucleophiles such as MeSH and MeNH$_2$ (see the Supporting Information). However, despite this reactivity profile and the stability in the presence of GSH (see the Supporting Information), the possibility of degrada-

tion of **21** with more complex and reactive endogenous nucleophiles such as protein thiols could not be excluded. Noteworthy, the position of the nitrile group oriented toward the iminium carbon is in agreement with the X-ray crystal structure of BASHY dye **21** (see Figure 4 and the Supporting Information). A steric clash between the substituents of the iminium carbon (R^1 = *i*-Bu) and phenylboronic acid (R^3 = *ortho*-CN) is detected, being consistent with the previously discussed interaction entailing the maximum width of the substituted phenyl ring of the boronic acid moiety and the minimum width of the *i*-Bu group. Furthermore, the computed Gibbs free energy of activation of 31.6 kcal mol^{-1} decreases to 27.7 and 24.0 kcal mol^{-1} by replacing the nitrile group by H in the phenyl boronic acid moiety and substituting *i*-Bu (R^1) by Et or H, respectively (see the Supporting Information). Indeed, this trend is consistent with the experimentally observed reduced hydrolytic stability of the dyes **4** and **6**.

The optical spectroscopic characteristics (see Figure 5A) of **21** in toluene confirm the photophysical integrity of the chromophore properties, regardless of the substitution pattern for R^1 or R^3; see data in the Supporting Information. Moreover, due to its hydrolytic stability, this dye was also characterized in 10 mM PBS (pH 7.4), containing 5% (v/v) DMF as cosolvent. As expected for a push−pull fluorophore, the absorption and fluorescence spectra in aqueous solution are red-shifted ($\lambda_{abs,max}$ = 504 nm, $\lambda_{f,max}$ = 562 nm) with respect to nonpolar toluene. For the fluorescence quantum yield (Φ_f) a value of 0.03 was determined. This value is considerably lower than observed in toluene (Φ = 0.67). As can be deduced from the tailing and slight broadening of the absorption spectrum, aggregation phenomena may play a role in aqueous solution. This provides a plausible explanation for the reduced fluorescence quantum yield.

Encouraged by the significant stability and favorable fluorescence properties of dye **21**, we performed the labeling of fixed HMC3 microglial cells. For comparison, dye **6** was used, having an Et substituent in the R^1 position and lacking the additional nitrile group at the boronic acid aryl moiety. As can be appreciated in the corresponding images in Figure 5B, the hydrolytically far less stable **6** ($t_{1/2}$ = 150 min) enables the observation of some emission 2.5 h after incubation. However, after 24 h only a very faint fluorescence signal was notable. On the contrary, dye **21** continues to show readily detectable emission after 24 h. The same observations were made qualitatively for the imaging of live A549 lung adenocarcinoma cells (see the Supporting Information). This result underpins that the mechanistic implications of the predicted hydrolytic stability are valid across several cell lines. Noteworthy, dye **21** presents low cytotoxicity against the two cell lines (IC$_{50}$ > 100 μM; see the Supporting Information), being negligible at the applied concentrations for the imaging experiments (typically 5−10 μM).

The stability of a chromophore defines the level of detail during bioimaging that would otherwise be lost during hydrolysis. This loss of information is not only restricted to steady-state confocal imaging, but also to the time-resolved component of the chromophore. The observed stability of the BASHY dye **21** enables the *in cellulo* investigation in live A549 lung adenocarcinoma cells via live-cell phasor fluorescence lifetime imaging microscopy (phasor-FLIM); see Figure 6.[57] Assisted by fit-free phasor analysis of photons obtained from time-correlated single-photon-counting (TCSPC), BASHY dye **21** exhibits two different fluorescence lifetime components,
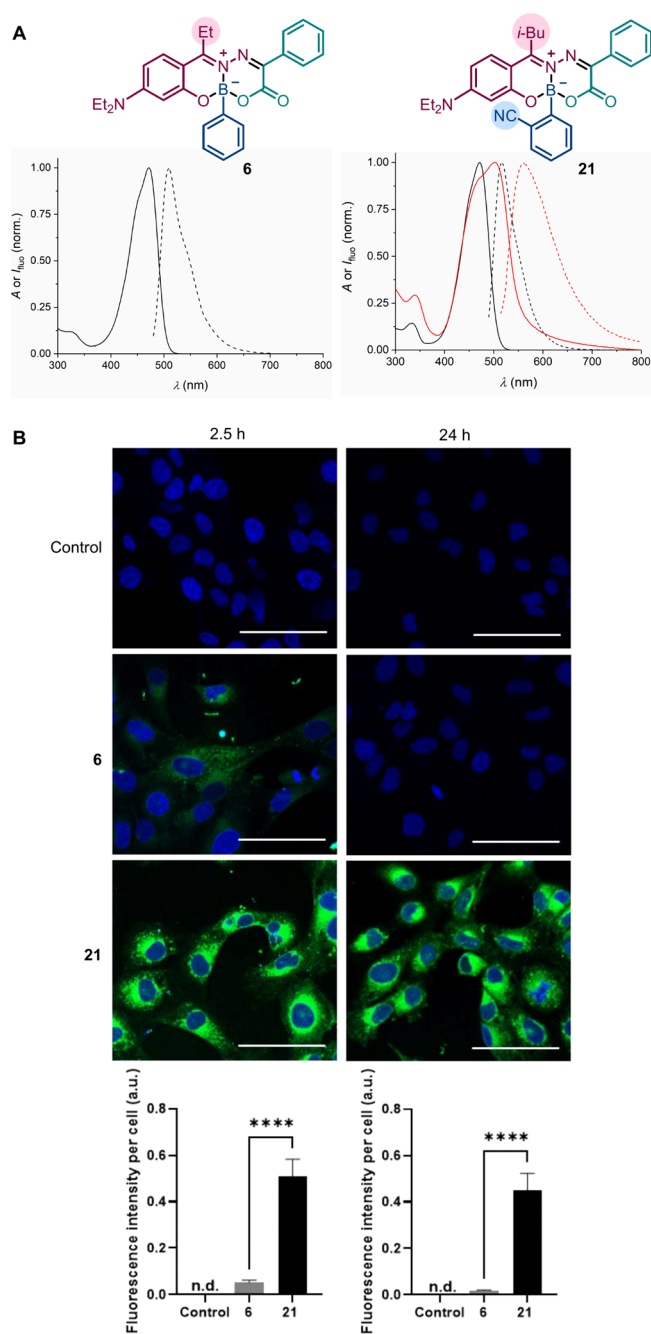

Figure 5. (A) UV/vis absorption (solid line) and fluorescence spectra (dashed line) of dye **6** (left) and **21** (right) in toluene (black) and PBS (pH 7.4, 5% (v/v) DMF as cosolvent; red); dye concentration *ca*. 10 μM. Note that for dye **6** no spectra in PBS were measured due to the instability of the compound. (B) Fluorescence microscopy images of fixed HMC3 microglial cells, incubated with the dyes **6** or **21**, after 2.5 and 24 h. Images show microglial cells with probe fluorescence (green) and nuclei staining with DAPI (blue). Graph bars represent the fluorescence intensity by cell (arbitrary units—a.u.) following analysis of images using ImageJ software. All images were acquired with the same fluorescence intensity gain at the confocal microscope and positive threshold defined equally for all images as 40. As shown dye **21** has a much higher fluorescence intensity than dye **6** for both 2.5h (p < 0.0001, ****) and 24h (p < 0.0001, ****) incubations, although a slight decrease of fluorescence is seen at 24 h. Scale bar: 100 μm.
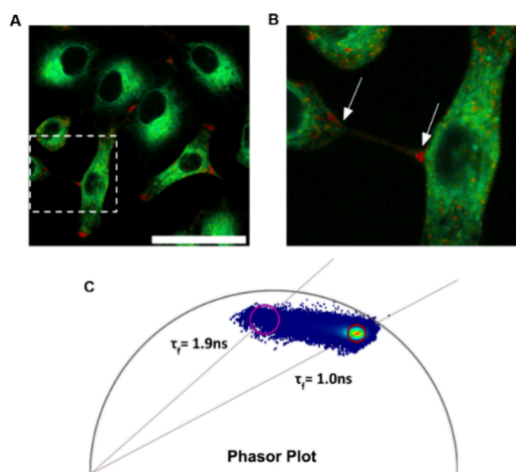
Figure 6. Phasor-FLIM of dye **21** in live A549 cells. (A) Phasor-FLIM image and separation of fluorescence lifetimes in the bulk (τ_f = 1.0 ns) and within vesicles (τ_f = 1.9 ns) after treatment with dye **21** at 4 h. (B) Zoomed image showing vesicle transport within tunneling nanotubes (white arrows) connecting between two living cells. Scale bar: 50 μm. (C) The spread of fluorescence lifetime across the phasor plot. The phasors are set to show the lifetimes of dye **21** in the cytosol and within intracellular vesicles.

namely in vesicles (1.0 ns) and around the perinuclear region (1.9 ns) (Figure 6C). Noteworthy, these lifetimes are different from the ones measured in PBS solution [biexponential decay: 1.62 ns (80%) and 6.48 ns (20%)]. Within cells, the heterogeneity in the microenvironment due to compartmentalization makes it substantially different from bulk water.[58] From the phasor plot, the linear spread of photons shows the dynamics of the dye and the spatial distribution/mixture between the two lifetimes within the cell. During time-lapsed capture, the vesicles associated with the shorter lifetime of **21** are of particular significance as they are observed to be transported within tunneling nanotubes as a form of cell-to-cell communication and content transfer (Figure 6B and video in the Supporting Information).[59]

With the aim of increasing the complexity of the biological object that is to be studied, we finally tested dye **21** in *in vivo* imaging studies of zebrafish larvae. The prolonged observation times and the fact that complete and complex organisms are imaged make the use of a dye with high chemical stability a mandatory choice. With this purpose, we determined the spatiotemporal distribution of **21** in 5 dpf zebrafish larvae exposed to the dye by immersion from 1 to 3 h (Figure 7 and the Supporting Information). Fish larvae were treated with the dye in a concentration range from 1 to 10 μM, without signs of toxicity as shown in brightfield images (malformation or edema). During the immersion, the fish were sampled at regular time points, anesthetized, and observed by *in vivo* fluorescence microscopy. From 1 h after incubation, the dye was taken up by zebrafish larvae and the fluorescent signal was mainly detected in the gastrointestinal tract, regardless of the concentration that was used (Figure 7). No fluorescence signal was visualized in the fish of the control group (only dimethyl sulfoxide, which was employed as vehicle for the dye application). At 1 μM, no fluorescence was observed outside the intestine. Interestingly, the fish larvae exposed to higher concentrations presented a wider straining pattern spread to the mouth (5 μM and 10 μM) and the throat (10 μM). At the highest concentration, the fluorescence signals reached the
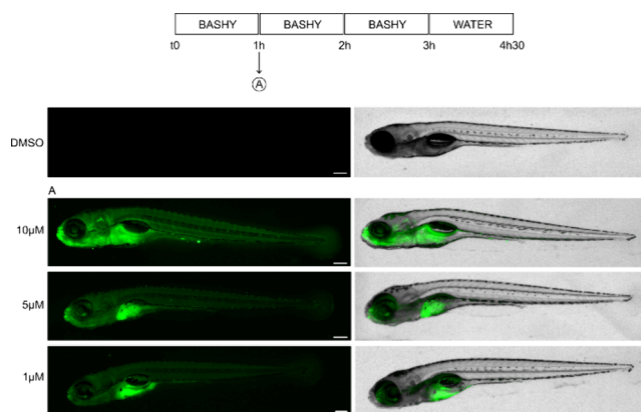
Figure 7. Five dpf zebrafish larvae vitally stained with dye **21**. Upper panel: Experimental design of fish labeling with dye **21**. Representative images (on the right side the brightfield images are shown) of zebrafish larvae immersed in a BASHY dye solution at 10 μM, 5 μM, and 1 μM. The control corresponds to the use of dimethyl sulfoxide (DMSO) without dye. Image acquisitions were performed after 1 h (A), 2 h (B) or 4.5 h (C; after 3 h the dye solution was substituted with water) of incubation. The images for the time points B and C are shown in the Supporting Information. Green fluorescent patterns of expression at the level of the whole body, mainly detected in the gastrointestinal tract, were observed. Scale bar: 200 μm.

entire fish body, however, at levels much lower than those observed in the digestive system. The dye was gradually taken up over time as the fluorescence signals increased between 1 and 2 h of immersion, without modification of the expression profiles. To evaluate the stability of the dye, the immersion time was extended to 3 h before dye removal. Even under those time-extended experimental settings, bright fluorescence signals were still detectable in the intestine of the larvae, including for those that were treated with the lowest dye concentration (1 μM).

CONCLUSIONS

A structurally diverse pool of fluorescent boronic acid derived salicylidenehydrazone (BASHY) complexes can be prepared with a versatile reaction protocol. The obtained set of compounds shows a large variation of the hydrolytic stability (half-life spanning from a few minutes to several days), which depends on steric and electronic factors, such as the alkyl substitution at the iminium carbon, the π-conjugation length, and the shielding by the aryl residue of the boronic acid component. The contributions of these effects were quantified by employing a mLFER model, which not only enabled a deeper understanding of the design requirements, but also led to the prediction of a new BASHY dye with significant hydrolytic resistance. The *in cellulo* stability of selected BASHY dyes was further evaluated in an iEDDA-based approach, providing independent validation to the structure−reactivity relationship. The predicted BASHY lead candidate **21** was successfully prepared and shown to be well-suited for bioimaging applications such as fluorescence lifetime imaging of live cells or *in vivo* fluorescence imaging of zebrafish larvae. The herein obtained results underpin the advantages of the modular BASHY platform with respect to the control of chemical stability and photophysical properties. These features label BASHY dyes as promising contenders for classical fluorescent dyes.

■ METHODOLOGY

Materials and Methods

Unless otherwise noted, reagents and solvents were used as received from commercial sources. Dichloromethane was dried using an INERT PureSolv Micro solvent purification system. Reagents used were purchased from Sigma-Aldrich. Thin-layer chromatography was performed using Merck silica gel 60 F$_{254}$ aluminum plates, visualized using UV light and revealed with phosphomolybdic acid solution. Silica gel for column (Geduran Si 60 0.040−0.063 mm) and for preparative thin layer chromatography (Silica gel 60 GF254) were purchased from Millipore.

NMR spectra were recorded with a Bruker Fourier 300 or 500 MHz using CDCl$_3$ or (CD$_3$)$_2$SO as deuterated solvents. All coupling constants are expressed in Hz and chemical shifts (δ) in ppm. The multiplicity is given as s (singlet), d (doublet), dd (double doublet), t (triplet), q (quartet) and m (multiplet). Low-resolution mass spectrometry (LRMS) was performed with an ion-trap mass analyzer (Thermo Scientific LCQ Fleet Ion Trap LC/MS) equipped with an electrospray interface and in a mass spectrometer (Micromass Quattro Micro API, Waters, Ireland) with a Triple Quadrupole (TQ) and with an electrospray ion source (ESI) operating in positive mode. High-resolution mass spectrometry (HRMS) was done with a Q Exactive Plus Hybrid Quadrupole Orbitrap Mass Spectrometer, using ESI in positive mode.

Hydrolytic Stability Studies of BASHY Dyes

The stability studies of the herein newly synthesized BASHY dyes were carried out at a concentration of 10 μM. For this a solution of the BASHY dye (60 μL of a 5 mM solution in DMF, 0.10 μmol) was added to PBS pH 7.4 (2.97 mL) at 21 °C and the UV/vis absorption spectra were recorded over time, following the decay of characteristic absorbance bands of BASHY.

Photophysical Measurements

The experiments were performed in 1-cm quartz cuvettes at room temperature (23 °C). The UV/vis absorption spectra were measured with a Cary 5000 UV/vis spectrophotometer (Varian) and corrected fluorescence emission spectra were obtained with a Varian Cary Eclipse fluorimeter, employing a pulsed xenon lamp for excitation. Lifetime measurements were performed using the time-correlated single-photon-counting technique (Edinburgh Instruments FLS 920). The samples were excited with a picosecond-pulsed EPLED 485 (482.0 nm, pulse width fwhm: 100.6 ps) and a Ludox solution was used to obtain the instrument response function. The kinetic decay curves were analyzed by deconvolution. The emission quantum yields were determined on optically diluted solutions (A ca. 0.1 at the excitation wavelength) and N-propyl-4-amino-1,8-naphthalimide was used as internal laboratory standard (Φ_f = 0.48 in aerated acetonitrile).[28] Different refractive indices of the solvents of the sample and the standard were taken into account.

Evaluation of the Stability of BASHY 21 in Different Conditions

BASHY 21 Half-Hife Determination in Dulbecco's Modified Eagle Medium. Method: 0.030 mL of BASHY 21 (1 mM in DMSO) were added to 2 mL of Dulbecco's Modified Eagle Medium (DMEM), 0.94 mL of ammonium acetate (20 mM; pH 7) and 30 μL of DMSO. Several time

points were analyzed using a Thermo Evolution 201 UV/vis Spectrophotometer.

Evaluation of BASHY 21 Stored in Wet-DMSO (5 mM) at 2−8 °C for 6 Months. Method: BASHY 21 (5 mM in DMSO) was analyzed using a Thermo Ultimate 3000 UPLC coupled with Q Exactive Plus Hybrid Quadrupole-Orbitrap mass spectrometer with ESI in the positive mode.

Evaluation of the Reaction of BASHY 21 with 10 equiv GSH (t = 24h). Method: 0.030 mL of BASHY 21 (1 mM in DMSO) were added to 2.64 mL of ammonium acetate (20 mM; pH 7), 0.300 mL of GSH (1 mM in H$_2$O) and 0.030 mL of DMSO. After 24 h, this assay was analyzed using a Thermo Ultimate 3000 UPLC coupled with Q-Exactive Plus Hybrid Quadrupole-Orbitrap mass spectrometer with electrospray ionization in the positive mode.

Evaluation of BASHY 21 Stability in Human Plasma. Method: 0.030 mL of BASHY 21 (1 mM in DMSO) were added to 2 mL of human plasma, 0.94 mL of ammonium acetate (20 mM; pH 7) and 0.030 mL of DMSO. Aliquots (0.2 mL) were taken at various time points and quenched with CH$_3$CN (0.2 mL) before analysis in a Thermo Ultimate 3000 UPLC coupled with a UV detector.

iEDDA Reaction of BASHY 15 and Its Hydrolysis Product

The reactions were carried out in the indicated solvent under pseudo first-order conditions in quartz cuvettes (1 cm path length; total volume approximately 3 mL) with solutions pre-equilibrated at room temperature (21 °C). Water (1.5 mL) and methanol (1.2 mL) were pipetted into the cuvette, followed by 3,6-di-2-pyridyl-1,2,4,5-tetrazine (Tz, final concentration of 333 μM, 150 μL from a stock solution in methanol) and dienophile (final concentrations of 450, 750, 1000, 1250, and 1500 μM, 150 μL from stock solutions in methanol). The pseudo first-order rate constants k_{obs} for the tetrazine reactions with an excess of alkene were determined. The decay of Tz absorbance (A) at 530 nm at 21 °C was plotted against time (s) for five different concentrations of the alkene. Triplicate independent measurements were carried out for the determination of k_{obs}. The second-order rate constant k_2 (M^{-1}s^{-1}) corresponds to the slope of calibration curves generated by plotting k_{obs} (s^{-1}) against the tetrazine concentration (M).

Data Analysis

DFT calculations and the development of the mLFER model are detailed in the Supporting Information.

DFT Study for the Hydrolysis of BASHY Dyes

Density functional theory (DFT) calculations were performed using the Gaussian software package[60] and structural representations were generated with CYLview.[61] All the geometry optimizations were carried out using the hybrid meta-GGA functional M06-2X developed by Truhlar and co-workers[62] and the valence double-ζ 6-31G(d,p) basis set. All optimized geometries were characterized by vibrational frequency calculations at the same level of theory as either minima (zero imaginary frequencies) or saddle points (single imaginary frequency) on the potential energy surface. For computation of the energy profiles, single-point energy calculations on the optimized geometries were then evaluated using the same functional and the valence triple-ζ def2-TZVPP basis set, with solvent effects (water) calculated by means of the Polarizable Continuum Model (PCM) initially devised by Tomasi and co-workers,[63−66] with radii and nonelectrostatic

terms of the SMD solvation model, developed by Truhler and co-workers.[67] The free energy values were derived from the electronic energy values obtained at the M06-2X/def2-TZVPP/SMD(water)//M06-2X/6-31G(d,p) level, and corrected by using the thermal and entropic corrections based on structural and vibration frequency data calculated at the M06-2X/6-31G(d,p) level of theory.

Fluorescence Imaging

Confocal Laser Scanning Microscopy and Fluorescence Lifetime Imaging Microscopy. CLSM-FLIM imaging was performed on a Stellaris 8 Leica DMi8 microscope (Leica Microsystems, S/N: 8300000313). The live-cell imaging was conducted in a microscope Incubator (Okolab). A549 Cells were cultured in an IBIDI-Treat 8-well chamber at a density of 20,000 cells per well in DMEM and allowed to adhere overnight at 37 °C, 5% CO_2. The medium was aspirated and BASHY dye **21** predissolved in DMEM at 5 μM was introduced. Incubation was performed at 37 °C, 5% CO_2. The cells were imaged live using an incubator-equipped Leica Stellaris 8 microscope (40× glycerol immersion objective) with fast lifetime contrast (FALCON) module. Samples were excited using a 40 MHz pulsed white light laser tuned to 520 nm (5.65% Laser Power) for both intensity and fluorescence lifetime measurements. Emitted photons were detected using HyD X (GaAsP hybrid photocathode) detector with a filter window at 535−660 nm. Fluorescence lifetime imaging (FLIM) was conducted with living cells at 4 min intervals, with scanning resolution of 1024 × 1024 pixels at 100 Hz, 3 frame accumulation equipped with adaptive focusing on each frame and well position. Acquisition was performed for 96 frame sets. Photons were counted based on FALCON-modified time-correlated single-photon-counting (TCSPC) method. Each pixel is transformed into a phasor plot

Culture of Human HMC3 Microglia Cell Line. Human HMC3 microglial cells were cultured in T75 culture flasks with 10 mL of growth medium consisting of Dulbecco's Modified Eagle's Medium (DMEM) supplemented with 10% FBS, 2% Antibiotic/Antimycotic (Sigma-Aldrich) and 1% L-glutamine (Sigma-Aldrich). T75 culture flasks were maintained in a humidified atmosphere containing 5% CO_2 at 37 °C. The growth media was changed every 2−3 days. To perform staining assays, cells were seeded onto 12-well noncoated plates for 24 h at a final concentration of 1×10^5 cells/mL.

Cell Incubation with BASHY Compounds. To assess the hydrolysis of BASHY, microglia were incubated with 2-vinylboronic acid (positive control) or BASHY dyes **15** and **17** for 1 h, after which, they were incubated with tetrazine-Cy5 for another hour. In another set of experiments to assess the significant stability and favorable fluorescence properties of BASHY dyes, HMC3 cells were incubated with dye **6** and **21** for 2.5 and 24 h. Following incubations, cells were fixed with 4% (w/v) PFA for 20 min at room temperature, washed three times with PBS and then cell nuclei was stained with DAPI; 1:1000 in PBS for 5 min, and the cells were washed three more times with PBS. In all staining procedures, the cells were kept in PBS for confocal microscopy, using a Leica DMi8-CS inverted microscope with Leica LAS X software.

Zebrafish Imaging

Zebrafish Husbandry. Animal experiments will be conducted at the fish facilities of IERP (building agreement n°C78−720) in compliance with the recommendations of Directive 2010−63-EU on the protection of animals used for

scientific purposes. Wild-type (AB strain) were raised in the IERP fish facility at INRAE Jouy-en-Josas. After spawning eggs were collected and incubated at 28 °C in E3 medium (5 mM NaCl, 0.17 mM KCl, 0.33 mM $CaCl_2$, 0.33 mM $MgSO_4$).

Zebrafish Staining and Imaging. BASHY dye **21** was dissolved in DMSO and sonicated to obtain a 5 mM stock solution. The stock solution was diluted in E3 media to prepare labeling solutions at 10 μM, 5 μM, and 1 μM. Zebrafish larvae were stained by immersion in a 10 μM, 5 μM or 1 μM **21** solution or an equivalent DMSO concentration for 1 h at 28 °C before dye removal by washing with E3 medium. Larvae were the anesthetized with MS222 diluted at 0.25 gL^{-1} in E3 media and mounted in a homemade observation chamber for fluorescence imaging. The fluorescence signals were acquired with an MZ10F stereomicroscope (Leica), equipped with a 0.63 × PLANAPO objective and a MC170HD camera (Leica).

■ ASSOCIATED CONTENT

Ⓢⓘ Supporting Information

The Supporting Information is available free of charge at https://pubs.acs.org/doi/10.1021/jacsau.4c00473.

> Synthesis, NMR and mass spectrometric data, X-ray crystal data, DFT calculations, additional microscopy images, details of the mLFER model, and its validation (PDF)
>
> Live cell FLIM (MP4)

■ AUTHOR INFORMATION

Corresponding Authors

Jaime A.S. Coelho − *Centro de Química Estrutural, Institute of Molecular Sciences, Faculty of Sciences, Universidade de Lisboa, Lisbon 1749-016, Portugal;* ⓞ orcid.org/0000-0002-7459-0993; Email: jaimeacoelho@edu.ulisboa.pt

Uwe Pischel − *CIQSO − Centre for Research in Sustainable Chemistry and Department of Chemistry, University of Huelva, Huelva 21071, Spain;* ⓞ orcid.org/0000-0001-8893-9829; Email: uwe.pischel@diq.uhu.es

Pedro M.P. Gois − *Research Institute for Medicines (iMed.ULisboa), Faculty of Pharmacy, Universidade de Lisboa, Lisbon 1649-003, Portugal;* ⓞ orcid.org/0000-0002-7698-630X; Email: pedrogois@ff.ulisboa.pt

Authors

João M.J.M. Ravasco − *Research Institute for Medicines (iMed.ULisboa), Faculty of Pharmacy, Universidade de Lisboa, Lisbon 1649-003, Portugal*

João Felicidade − *Research Institute for Medicines (iMed.ULisboa), Faculty of Pharmacy, Universidade de Lisboa, Lisbon 1649-003, Portugal*

Maria V. Pinto − *Research Institute for Medicines (iMed.ULisboa), Faculty of Pharmacy, Universidade de Lisboa, Lisbon 1649-003, Portugal*

Fábio M.F. Santos − *Research Institute for Medicines (iMed.ULisboa), Faculty of Pharmacy, Universidade de Lisboa, Lisbon 1649-003, Portugal*

René Campos-González − *CIQSO − Centre for Research in Sustainable Chemistry and Department of Chemistry, University of Huelva, Huelva 21071, Spain*

Jesús F. Arteaga − *CIQSO − Centre for Research in Sustainable Chemistry and Department of Chemistry,*

University of Huelva, Huelva 21071, Spain; ● orcid.org/
0000-0001-8153-6621

Manon Mehraz − *INRAE National Research Institute for
Agriculture, Food and Environment, Université Paris-Saclay,
Jouy-en-Josas 78350, France*

Christelle Langevin − *INRAE National Research Institute for
Agriculture, Food and Environment, Université Paris-Saclay,
Jouy-en-Josas 78350, France;* ● orcid.org/0000-0002-6013-
4460

Adelaide Fernandes − *Research Institute for Medicines
(iMed.ULisboa), Faculty of Pharmacy, Universidade de
Lisboa, Lisbon 1649-003, Portugal;* ● orcid.org/0000-
0002-2782-9519

Ha-Chi Nguyen − *Max Planck Institute for Polymer Research,
Mainz 55128, Germany*

David Y.W. Ng − *Max Planck Institute for Polymer Research,
Mainz 55128, Germany;* ● orcid.org/0000-0002-0302-
0678

Complete contact information is available at:
https://pubs.acs.org/10.1021/jacsau.4c00473

Author Contributions

J.M.J.M. Ravasco: methodology, investigations-experiments, writing—initial draft. J. Felicidade, M.V. Pinto, F.M.F. Santos, R. González-Campos, J.F. Arteaga, M. Mehraz, H.-C. Nguyen: investigations—experiments. A. Fernandes, C. Langevin, D.Y.W. Ng: supervision, writing—review and editing, funding acquisition. J.A.S. Coelho: methodology, formal analysis, data treatment, writing—review and editing. U. Pischel: supervision, funding acquisition, writing—final draft, review, and editing. P.M.P. Gois: supervision, funding acquisition, writing—review and editing, project administration. CRediT: **João M. J. M. Ravasco** investigation; **João Felicidade** investigation; **Maria V. Pinto** investigation; **Fábio M. F. Santos** investigation; **René González-Campos** investigation; **Jesús F. Arteaga** investigation; **Manon Mehraz** investigation; **Christelle Langevin** conceptualization, investigation; **Adelaide Fernandes** conceptualization, investigation; **Ha-Chi Nguyen** investigation; **David Y.W. Ng** conceptualization; **Jaime A. S. Coelho** conceptualization, investigation, writing - review & editing; **Uwe Pischel** conceptualization, writing - original draft, writing - review & editing; **Pedro M. P. Gois** conceptualization, supervision, writing - original draft, writing - review & editing.

Notes

The authors declare no competing financial interest.

REFERENCES

(1) Lavis, L. D.; Raines, R. T. Bright Building Blocks for Chemical Biology. *ACS Chem. Biol.* **2014**, *9*, 855−866.

(2) Xu, W.; Zeng, Z.; Jiang, J.-H.; Chang, Y.-T.; Yuan, L. Discerning the Chemistry in Individual Organelles with Small-Molecule Fluorescent Probes. *Angew. Chem., Int. Ed.* **2016**, *55*, 13658−13699.

(3) Klymchenko, A. S. Solvatochromic and Fluorogenic Dyes as Environment-Sensitive Probes: Design and Biological Applications. *Acc. Chem. Res.* **2017**, *50*, 366−375.

(4) Lavis, L. D. Chemistry Is Dead. Long Live Chemistry! *Biochemistry* **2017**, *56*, 5165−5170.

(5) Benson, S.; De Moliner, F.; Tipping, W.; Vendrell, M. Miniaturized Chemical Tags for Optical Imaging. *Angew. Chem., Int. Ed.* **2022**, *61*, No. e202204788.

(6) Renikuntla, B. R.; Rose, H. C.; Eldo, J.; Waggoner, A. S.; Armitage, B. A. Improved Photostability and Fluorescence Properties through Polyfluorination of a Cyanine Dye. *Org. Lett.* **2004**, *6*, 909−912.

(7) Peng, X.; Song, F.; Lu, E.; Wang, Y.; Zhou, W.; Fan, J.; Gao, Y. Heptamethine Cyanine Dyes with a Large Stokes Shift and Strong Fluorescence: A Paradigm for Excited-State Intramolecular Charge Transfer. *J. Am. Chem. Soc.* **2005**, *127*, 4170−4171.

(8) Loudet, A.; Burgess, K. BODIPY dyes and their derivatives: syntheses and spectroscopic properties. *Chem. Rev.* **2007**, *107*, 4891−4932.

(9) Beija, M.; Afonso, C. A. M.; Martinho, J. M. G. Synthesis and applications of Rhodamine derivatives as fluorescent probes. *Chem. Soc. Rev.* **2009**, *38*, 2410−2433.

(10) Samanta, A.; Vendrell, M.; Das, R.; Chang, Y. T. Development of Photostable Near-Infrared Cyanine Dyes. *Chem. Commun.* **2010**, *46*, 7406−7408.

(11) Vendrell, M.; Zhai, D.; Er, J. C.; Chang, Y.-T. Combinatorial strategies in fluorescent probe development. *Chem. Rev.* **2012**, *112*, 4391−4420.

(12) Grimm, J. B.; Sung, A. J.; Legant, W. R.; Hulamm, P.; Matlosz, S. M.; Betzig, E.; Lavis, L. D. Carbofluoresceins and Carborhodamines as Scaffolds for High Contrast Fluorogenic Probes. *ACS Chem. Biol.* **2013**, *8*, 1303−1310.

(13) Frath, D.; Massue, J.; Ulrich, G.; Ziessel, R. Luminescent materials: locking π-conjugated and heterocyclic ligands with boron(III). *Angew. Chem., Int. Ed.* **2014**, *53*, 2290−2310.

(14) Grimm, J. B.; English, B. P.; Chen, J.; Slaughter, J. P.; Zhang, Z.; Revyakin, A.; Patel, R.; Macklin, J. J.; Normanno, D.; Singer, R. H.; Lionnet, T.; Lavis, L. D. A general method to improve fluorophores for live-cell and single-molecule spectroscopy. *Nat. Methods* **2015**, *12*, 244−250.

(15) Kushida, Y.; Nagano, T.; Hanaoka, K. Silicon-substituted xanthene dyes and their applications in bioimaging. *Analyst* **2015**, *140*, 685−695.

(16) Pais, V. F.; Alcaide, M. M.; López-Rodríguez, R.; Collado, D.; Nájera, F.; Pérez-Inestrosa, E.; Álvarez, E.; Lassaletta, J. M.; Fernández, R.; Ros, A.; Pischel, U. Strongly Emissive and Photostable Four-Coordinate Organoboron *N,C* Chelates and Their Use in Fluorescence Microscopy. *Chem. - Eur. J.* **2015**, *21*, 15369−15376.

(17) Kolmakov, K.; Hebisch, E.; Wolfram, T.; Nordwig, L. A.; Wurm, C. A.; Ta, H.; Westphal, V.; Belov, V. N.; Hell, S. W. Far-Red Emitting Fluorescent Dyes for Optical Nanoscopy: Fluorinated Silicon-Rhodamines (SiRF Dyes) and Phosphorylated Oxazines. *Chem. - Eur. J.* **2015**, *21*, 13344−13356.

(18) Collot, M.; Fam, T. K.; Ashokkumar, P.; Faklaris, O.; Galli, T.; Danglot, L.; Klymchenko, A. S. Ultrabright and Fluorogenic Probes for Multicolor Imaging and Tracking of Lipid Droplets in Cells and Tissues. *J. Am. Chem. Soc.* **2018**, *140*, 5401−5411.

(19) Heynck, L.; Matthias, J.; Bossi, M. L.; Butkevich, A. N.; Hell, S. W. *N*-Cyanorhodamines: cell-permeant, photostable and bathochromically shifted analogues of fluoresceins. *Chem. Sci.* **2022**, *13*, 8297−8306.

(20) Jiang, G.; Ren, T.-B.; D'Este, E.; Xiong, M.; Xiong, B.; Johnsson, K.; Zhang, X.-B.; Wang, L.; Yuan, L. A synergistic strategy to develop photostable and bright dyes with long Stokes shift for nanoscopy. *Nat. Commun.* **2022**, *13*, 2264.

(21) Grimm, J. B.; Tkachuk, A. N.; Patel, R.; Hennigan, S. T.; Gutu, A.; Dong, P.; Gandin, V.; Osowski, A. M.; Holland, K. L.; Liu, Z. J.; Brown, T. A.; Lavis, L. D. Optimized Red-Absorbing Dyes for Imaging and Sensing. *J. Am. Chem. Soc.* **2023**, *145*, 23000−23013.

(22) Yang, T.; Valavalkar, A.; Romero-Arenas, A.; Dasgupta, A.; Then, P.; Chettri, A.; Eggeling, C.; Ros, A.; Pischel, U.; Dietzek-Ivanšić, B. Excited-State Dynamics in Borylated Arylisoquinoline Complexes in Solution and *in cellulo*. *Chem. - Eur. J.* **2023**, *29*, No. e202203468.

(23) Vázquez-Romero, A.; Kielland, N.; Arévalo, M. J.; Preciado, S.; Mellanby, R. J.; Feng, Y.; Lavilla, R.; Vendrell, M. Multicomponent Reactions for *de Novo* Synthesis of BODIPY Probes: *In Vivo* Imaging of Phagocytic Macrophages. *J. Am. Chem. Soc.* **2013**, *135*, 16018−16021.

(24) de Moliner, F.; Kielland, N.; Lavilla, R.; Vendrell, M. Modern Synthetic Avenues for the Preparation of Functional Fluorophores. *Angew. Chem., Int. Ed.* **2017**, *56*, 3758−3769.

(25) Fernandez, A.; Kielland, N.; Makda, A.; Carragher, N. O.; González-García, M. C.; Espinar-Barranco, L.; González-Vera, J. A.; Orte, A.; Lavilla, R.; Vendrell, M. A multicomponent reaction platform towards multimodal near-infrared BODIPY dyes for STED and fluorescence lifetime imaging. *RSC Chem. Biol.* **2022**, *3*, 1251−1259.

(26) Levi, L.; Müller, T. J. J. Multicomponent syntheses of functional chromophores. *Chem. Soc. Rev.* **2016**, *45*, 2825−2846.

(27) Levi, L.; Müller, T. J. J. Multicomponent Syntheses of Fluorophores Initiated by Metal Catalysis. *Eur. J. Org. Chem.* **2016**, 2902−2918.

(28) Santos, F. M. F.; Rosa, J. N.; Candeias, N. R.; Carvalho, C. P.; Matos, A. I.; Ventura, A. E.; Florindo, H. F.; Silva, L. C.; Pischel, U.; Gois, P. M. P. A Three-Component Assembly Promoted by Boronic Acids Delivers a Modular Fluorophore Platform (BASHY Dyes). *Chem. - Eur. J.* **2016**, *22*, 1631−1637.

(29) Alcaide, M. M.; Santos, F. M. F.; Pais, V. F.; Carvalho, J. I.; Collado, D.; Pérez-Inestrosa, E.; Arteaga, J. F.; Boscá, F.; Gois, P. M. P.; Pischel, U. Electronic and Functional Scope of Boronic Acid Derived Salicylidenehydrazone (BASHY) Complexes as Fluorescent Dyes. *J. Org. Chem.* **2017**, *82*, 7151−7158.

(30) Cal, P. M. S. D.; Sieglitz, F.; Santos, F. M. F.; Parente Carvalho, C.; Guerreiro, A.; Bertoldo, J. B.; Pischel, U.; Gois, P. M. P.; Bernardes, G. J. L. Site-selective installation of BASHY fluorescent dyes to Annexin V for targeted detection of apoptotic cells. *Chem. Commun.* **2017**, *53*, 368−371.

(31) Santos, F. M. F.; Domínguez, Z.; Fernandes, J. P. L.; Parente Carvalho, C.; Collado, D.; Pérez-Inestrosa, E.; Pinto, M. V.; Fernandes, A.; Arteaga, J. F.; Pischel, U.; Gois, P. M. P. Cyanine-like boronic acid derived salicylidenehydrazone complexes (Cy-BASHY) for bioimaging applications. *Chem. - Eur. J.* **2020**, *26*, 14064−14069.

(32) Pinto, M. V.; Santos, F. M. F.; Barros, C.; Ribeiro, A. R.; Pischel, U.; Gois, P. M. P.; Fernandes, A. BASHY dye platform enables the fluorescence bioimaging of myelin debris phagocytosis by microglia during demyelination. *Cells* **2021**, *10*, 3163−3182.

(33) Baldo, S.; Antunes, P.; Felicidade, J. F.; Santos, F. M. F.; Arteaga, J. F.; Fernandes, F.; Pischel, U.; Pinto, S. N.; Gois, P. M. P. The BASHY platform enables the assembly of a fluorescent bortezomib-GV1001 conjugate. *ACS Med. Chem. Lett.* **2022**, *13*, 128−133.

(34) Felicidade, J.; Santos, F. M. F.; Arteaga, J. F.; Remón, P.; Campos-González, R.; Nguyen, H.-C.; Nájera, F.; Boscá, F.; Ng, D. Y. W.; Gois, P. M. P.; Pischel, U. Engineering the BASHY dye platform toward architectures with responsive fluorescence. *Chem. - Eur. J.* **2023**, *29*, No. e202300579.

(35) de Almeida, A. F.; Moreira, R.; Rodrigues, T. Synthetic Organic Chemistry Driven by Artificial Intelligence. *Nat. Rev. Chem.* **2019**, *3*, 589−604.

(36) Hueffel, J. A.; Sperger, T.; Funes-Ardoiz, I.; Ward, J. A.; Rissanen, K.; Schoenebeck, F. Accelerated dinuclear palladium catalyst identification through unsupervised machine learning. *Science* **2021**, *374*, 1134−1140.

(37) Jorner, K.; Tomberg, A.; Bauer, C.; Sköld, C.; Norrby, P.-O. Organic reactivity from mechanism to machine learning. *Nat. Rev. Chem.* **2021**, *5*, 240−255.

(38) Williams, W. L.; Zeng, L.; Gensch, T.; Sigman, M. S.; Doyle, A. G.; Anslyn, E. V. The Evolution of Data-Driven Modeling in Organic Chemistry. *ACS Central Sci.* **2021**, *7*, 1622−1637.

(39) Zhang, S.-Q.; Xu, L.-C.; Li, S.-W.; Oliveira, J. C. A.; Li, X.; Ackermann, L.; Hong, X. Bridging Chemical Knowledge and Machine Learning for Performance Prediction of Organic Synthesis. *Chem. - Eur. J.* **2023**, *29*, No. e202202834.

(40) Santiago, C. B.; Guo, J.-Y.; Sigman, M. S. Predictive and Mechanistic Multivariate Linear Regression Models for Reaction Development. *Chem. Sci.* **2018**, *9*, 2398−2412.

(41) Crawford, J. M.; Kingston, C.; Toste, F. D.; Sigman, M. S. Data Science Meets Physical Organic Chemistry. *Acc. Chem. Res.* **2021**, *54*, 3136−3148.

(42) Ravasco, J. M. J. M.; Coelho, J. A. S. Predictive Multivariate Models for Bioorthogonal Inverse-Electron Demand Diels-Alder Reactions. *J. Am. Chem. Soc.* **2020**, *142*, 4235−4241.

(43) Dotson, J. J.; Anslyn, E. V.; Sigman, M. S. A Data-Driven Approach to the Development and Understanding of Chiroptical Sensors for Alcohols with Remote γ-Stereocenters. *J. Am. Chem. Soc.* **2021**, *143*, 19187−19198.

(44) Griffin, J. D.; Pancoast, A. R.; Sigman, M. S. Interrogation of 2,2′-Bipyrimidines as Low-Potential Two-Electron Electrolytes. *J. Am. Chem. Soc.* **2021**, *143*, 992−1004.

(45) Haas, B. C.; Goetz, A. E.; Bahamonde, A.; McWilliams, J. C.; Sigman, M. S. Predicting relative efficiency of amide bond formation using multivariate linear regression. *Proc. Natl. Acad. Sci. U. S. A.* **2022**, *119*, No. e2118451119.

(46) Xu, E. Y.; Werth, J.; Roos, C. B.; Bendelsmith, A. J.; Sigman, M. S.; Knowles, R. R. Noncovalent Stabilization of Radical Intermediates in the Enantioselective Hydroamination of Alkenes with Sulfonamides. *J. Am. Chem. Soc.* **2022**, *144*, 18948−18958.

(47) Rein, J.; Meinhardt, J. M.; Hofstra Wahlman, J. L.; Sigman, M. S.; Lin, S. A Physical Organic Approach towards Statistical Modeling of Tetrazole and Azide Decomposition. *Angew. Chem., Int. Ed.* **2023**, *62*, No. e202218213.

(48) Zhao, S.; Gensch, T.; Murray, B.; Niemeyer, Z. L.; Sigman, M. S.; Biscoe, M. R. Enantiodivergent Pd-Catalyzed C−C Bond Formation Enabled through Ligand Parameterization. *Science* **2018**, *362*, 670−674.

(49) Kelly, S. P.; Shende, V. V.; Flynn, A. R.; Dan, Q.; Ye, Y.; Smith, J. L.; Tsukamoto, S.; Sigman, M. S.; Sherman, D. H. Data Science-Driven Analysis of Substrate-Permissive Diketopiperazine Reverse Prenyltransferase NotF: Applications in Protein Engineering and Cascade Biocatalytic Synthesis of (−)-Eurotiumin A. *J. Am. Chem. Soc.* **2022**, *144*, 19326−19336.

(50) Nistanaki, S. K.; Williams, C. G.; Wigman, B.; Wong, J. J.; Haas, B. C.; Popov, S.; Werth, J.; Sigman, M. S.; Houk, K. N.; Nelson, H. M.

Catalytic asymmetric C-H insertion reactions of vinyl carbocations. *Science* **2022**, *378*, 1085−1091.

(51) Clements, H. D.; Flynn, A. R.; Nicholls, B. T.; Grosheva, D.; Lefave, S. J.; Merriman, M. T.; Hyster, T. K.; Sigman, M. S. Using Data Science for Mechanistic Insights and Selectivity Predictions in a Non-Natural Biocatalytic Reaction. *J. Am. Chem. Soc.* **2023**, *145*, 17656−17664.

(52) Liles, J. P.; Rouget-Virbel, C.; Wahlman, J. L. H.; Rahimoff, R.; Crawford, J. M.; Medlin, A.; O'Connor, V. S.; Li, J.; Roytman, V. A.; Toste, F. D.; Sigman, M. S. Data science enables the development of a new class of chiral phosphoric acid catalysts. *Chem.* **2023**, *9*, 1518−1537.

(53) Tang, T.; Hazra, A.; Min, D. S.; Williams, W. L.; Jones, E.; Doyle, A. G.; Sigman, M. S. Interrogating the Mechanistic Features of Ni(I)-Mediated Aryl Iodide Oxidative Addition Using Electroanalytical and Statistical Modeling Techniques. *J. Am. Chem. Soc.* **2023**, *145*, 8689−8699.

(54) Saridakis, I.; Riomet, M.; Belleza, O. J. V.; Coussanes, G.; Singer, N. K.; Kastner, N.; Xiao, Y.; Smith, E.; Tona, V.; De la Torre, A.; Lopes, E. F.; Sánchez-Murcia, P. A.; González, L.; Sitte, H. H.; Maulide, N. PyrAtes: Modular Organic Salts with Large Stokes Shifts for Fluorescence Microscopy. *Angew. Chem., Int. Ed.* **2024**, *63*, No. e202318127.

(55) Laurent, A. D.; Le Guennic, B.; Jacquemin, D. Theoretical spectroscopy of BASHY dyes. *Theor. Chem. Acc.* **2016**, *135*, 173.

(56) Silva, M. J. S. A.; Zhang, Y.; Vinck, R.; Santos, F. M. F.; António, J. P. M.; Gourdon-Grünewaldt, L.; Zaouter, C.; Castonguay, A.; Patten, S. A.; Cariou, K.; Boscá, F.; Nájera, F.; Arteaga, J. F.; Gasser, G.; Pischel, U.; Gois, P. M. P. BASHY Dyes Are Highly Efficient Lipid Droplet-Targeting Photosensitizers that Induce Ferroptosis through Lipid Peroxidation. *Bioconjugate Chem.* **2023**, *34*, 2337−2344.

(57) Stringari, C.; Cinquin, A.; Cinquin, O.; Digman, M. A.; Donovan, P. J.; Gratton, E. Phasor approach to fluorescence lifetime microscopy distinguishes different metabolic states of germ cells in a live tissue. *Proc. Natl. Acad. Sci. U.S.A.* **2011**, *108*, 13582−13587.

(58) Antifeeva, I. A.; Fonin, A. V.; Feflova, A. S.; Stepanenko, O. V.; Povarova, O. I.; Silonov, S. A.; Kuznetsova, I. M.; Uversky, V. N.; Turoverov, K. K. Liquid-liquid phase separation as an organizing principle of intracellular space: overview of the evolution of the cell compartmentalization concept. *Cell. Mol. Life Sci.* **2022**, *79*, 251−282.

(59) Rustom, A.; Saffrich, R.; Markovic, I.; Walther, P.; Gerdes, H.-H. Nanotubular Highways for Intercellular Organelle Transport. *Science* **2004**, *303*, 1007−1010.

(60) Frisch, M. J.; Trucks, G. W.; Schlegel, H. B.; Scuseria, G. E.; Robb, M. A.; Cheeseman, J. R.; Scalmani, G.; Barone, V.; Petersson, G. A.; Nakatsuji, H.; Li, X.; Caricato, M.; Marenich, A. V.; Bloino, J.; Janesko, B. G.; Gomperts, R.; Mennucci, B.; Hratchian, H. P.; Ortiz, J. V.; Izmaylov, A. F.; Sonnenberg, J. L.; Williams-Young, D.; Ding, F.; Lipparini, F.; Egidi, F.; Goings, J.; Peng, B.; Petrone, A.; Henderson, T.; Ranasinghe, D.; Zakrzewski, V. G.; Gao, J.; Rega, N.; Zheng, G.; Liang, W.; Hada, M.; Ehara, M.; Toyota, K.; Fukuda, R.; Hasegawa, J.; Ishida, M.; Nakajima, T.; Honda, Y.; Kitao, O.; Nakai, H; Vreven, T.; Throssell, K.; Montgomery, J. A., Jr.; Peralta, J. E.; Ogliaro, F.; Bearpark, M. J.; Heyd, J. J.; Brothers, E. N.; Kudin, K. N.; Staroverov, V. N.; Keith, T. A.; Kobayashi, R.; Normand, J.; Raghavachari, K.; Rendell, A. P.; Burant, J. C.; Iyengar, S. S.; Tomasi, J.; Cossi, M.; Millam, J. M.; Klene, M; Adamo, C.; Cammi, R.; Ochterski, J. W.; Martin, R. L.; Morokuma, K.; Farkas, O.; Foresman, J. B.; Fox, D. J. *Gaussian 16*, (Revision C.01), Gaussian, Inc.: Wallingford, CT, 2019

(61) CYLview20; Legault, C. Y. Université de Sherbrooke, 2020 (http://www.cylview.org).

(62) Zhao, Y.; Truhlar, D. G. The M06 suite of density functionals for main group thermochemistry, thermochemical kinetics, non-covalent interactions, excited states, and transition elements: two new functionals and systematic testing of four M06-class functionals and 12 other functionals. *Theor. Chem. Acc.* **2008**, *120*, 215−241.

(63) Cancès, E.; Mennucci, B.; Tomasi, J. A new integral equation formalism for the polarizable continuum model: Theoretical back-ground and applications to isotropic and anisotropic dielectrics. *J. Chem. Phys.* **1997**, *107*, 3032−3041.

(64) Cossi, M.; Barone, V.; Mennucci, B.; Tomasi, J. Ab initio study of ionic solutions by a polarizable continuum dielectric model. *Chem. Phys. Lett.* **1998**, *286*, 253−260.

(65) Tomasi, J.; Mennucci, B.; Cammi, R. Quantum Mechanical Continuum Solvation Models. *Chem. Rev.* **2005**, *105*, 2999−3094.

(66) Marenich, A. V. Universal Solvation Model Based on Solute Electron Density and on a Continuum Model of the Solvent Defined by the Bulk Dielectric Constant and Atomic Surface Tensions. *J. Phys. Chem. B.* **2009**, *113*, 6378−6396.

(67) Marenich, A. V.; Cramer, C. J.; Truhlar, D. G. Universal Solvation Model Based on Solute Electron Density and on a Continuum Model of the Solvent Defined by the Bulk Dielectric Constant and Atomic Surface Tensions. *J. Phys. Chem. B.* **2009**, *113*, 6378−6396.